



# Remarkably boosting catalytic H<sub>2</sub> evolution from ammonia borane through the visible-light-driven synergistic electron effect of non-plasmonic noble-metal-free nanoparticles and photoactive metal-organic frameworks

Jin Song, Xiaojun Gu\*, Jia Cheng, Na Fan, Hao Zhang, Haiquan Su\*

Inner Mongolia Key Laboratory of Coal Chemistry, School of Chemistry and Chemical Engineering, Inner Mongolia University, Hohhot, 010021, China



## ARTICLE INFO

**Keywords:**  
H<sub>2</sub> evolution  
Noble-metal-free nanoparticles  
Photoactive metal-organic frameworks  
Synergistic electron effect

## ABSTRACT

From the viewpoint of regulating and enriching the electron density of noble-metal-free nanoparticles (NPs) to remarkably enhance their catalytic activities in the reduction-dominated reactions, we synthesized a series of non-plasmonic Co and Ni nanoparticles (NPs) supported by NH<sub>2</sub>-functionalized photoactive and NH<sub>2</sub>-free non-photoactive metal-organic frameworks (MOFs) with different compositions and framework structures, which were used to catalyze H<sub>2</sub> evolution from ammonia borane (NH<sub>3</sub>BH<sub>3</sub>) in aqueous solution under visible light irradiation at 298 K. The systematic investigation showed that the catalysts containing photoactive MOFs had higher activities than those containing non-photoactive MOFs under visible light irradiation though the photocatalytic activities of all the catalysts were enhanced in comparison with the activities in the dark. Specifically, the Co catalysts containing photoactive MOFs had the total turnover frequency (TOF) values in the range of 81.7–117.7 min<sup>-1</sup>, which were much higher than the values of reported noble-metal-free catalysts and were even comparable to the values of noble metal catalysts. The remarkably enhanced activities of the supported catalysts could be attributed to the visible-light-driven synergistic electron effect of semiconductor-like MOFs and non-plasmonic noble-metal-free NPs, which was verified by the increased photocurrent density of Co/MIL-101(Cr)-NH<sub>2</sub>. Moreover, the catalysts still had 100% of H<sub>2</sub> selectivity and high activities after 25 runs of catalysis.

## 1. Introduction

Currently, searching hydrogen storage materials and methods for high-energy-density H<sub>2</sub> evolution in safe and efficient ways is urgently required toward the fuel-cell-based hydrogen economy [1–3]. Ammonia borane (NH<sub>3</sub>BH<sub>3</sub>) with high hydrogen content (19.6 wt%) is regarded as one of the leading chemical hydrogen storage materials [4–6]. Although various heterogeneous metal catalysts can promote the release of H<sub>2</sub> from NH<sub>3</sub>BH<sub>3</sub> (NH<sub>3</sub>BH<sub>3</sub> + 2H<sub>2</sub>O → NH<sub>4</sub>BO<sub>2</sub> + 3H<sub>2</sub>), the development of non-noble metal catalysts such as supported Co and Ni nanoparticles (NPs) with high activities is highly desirable but still remains a big challenge [7–31]. It has been widely approved that decreasing the sizes of metal NPs through the utilization of porous supports benefits their catalytic activity enhancement [32–34]. Besides this method, regulating and enriching the electronic density of metal NPs in the catalysts through tuning the interaction between metal and support or constructing heterometallic NPs with alloy or core-shell structures seems more effective to realize this objective [35–38]. However, the activity gap between non-noble and noble metal catalysts is still large

[7–31]. Thus, exploring other methods to remarkably enhance the electron density of non-noble metal NPs is desired and urgent for the H<sub>2</sub>-generated application of NH<sub>3</sub>BH<sub>3</sub>, especially in the portable and on-demand fields.

Solar light can be used as driving force to enrich the electron density of catalytically active metal NPs [39–43]. Recently, it has been found that the interband electron transitions of non-plasmonic metal NPs such as Pt, Rh, Co and Ni can result in the formation of excited electrons under light irradiation [44–48]. So we deduce that if the non-plasmonic Co and Ni NPs are used in catalytic H<sub>2</sub> evolution from NH<sub>3</sub>BH<sub>3</sub> under visible light irradiation, their electron density could be enriched and then their activities would be enhanced. However, the single interband electron transition induced by the light absorption, especially the visible light absorption, often leads to that the electron density of non-plasmonic metal NPs is not high enough for the remarkable enhancement of catalytic activity [44–48]. Therefore, in order to further enhance their photogenerated electron density, selecting photoactive species to support non-plasmonic metal NPs becomes necessary. Among various photoactive species, some metal-organic frameworks (MOFs)

\* Corresponding authors.

E-mail addresses: [xiaojun.gu@yahoo.com](mailto:xiaojun.gu@yahoo.com) (X. Gu), [haiquansu@yahoo.com](mailto:haiquansu@yahoo.com), [haiquansu@sina.com](mailto:haiquansu@sina.com) (H. Su).

exhibit the semiconductor-like behaviors under visible light irradiation due to the delocalization and excitation of the electrons from the highest occupied molecular orbital (HOMO) to the lowest unoccupied molecular orbital (LUMO) state of organic linkers containing amine or porphyrin groups [49–62]. More importantly, these hot electrons can be further transferred to the non-plasmonic metal NPs in the MOF-supported catalysts. In addition, the well-defined crystalline structures of photoactive MOFs are useful for elucidating the structure–performance relationships of resultant photocatalysts [49–68]. On the basis of the above considerations, it could be envisioned that if photoactive MOFs are used to support non-plasmonic noble-metal-free NPs, their electron density would be remarkably enhanced through the synergistic electron contribution of themselves and photoactive MOFs under visible light irradiation, which could lead to the remarkably enhanced activities in the reduction-dominated catalytic reactions including H<sub>2</sub> evolution from NH<sub>3</sub>BH<sub>3</sub>.

Herein, we reported a series of non-plasmonic Co and Ni NPs supported by four NH<sub>2</sub>-functionalized photoactive MOFs (MIL-101(Cr)-NH<sub>2</sub>, MIL-101(Al)-NH<sub>2</sub>, MIL-53(Cr)-NH<sub>2</sub> and MIL-53(Al)-NH<sub>2</sub>) and three NH<sub>2</sub>-free non-photoactive MOFs (MIL-101(Cr), MIL-53(Cr) and MIL-53(Al)), which were used as catalysts for H<sub>2</sub> evolution from NH<sub>3</sub>BH<sub>3</sub> in aqueous solution under visible light irradiation at 298 K. Interestingly, compared with the activities of all the catalysts in the dark, their visible-light-driven activities were enhanced and the catalysts based on photoactive MOFs had much higher activities than the catalysts based on non-photoactive MOFs. Particularly, the Co NPs supported by photoactive MOFs exhibited the highest total turnover frequency (TOF) values in the range of 81.7–117.7 min<sup>-1</sup>. Moreover, the influences of the visible light intensity and the electron density of metal NPs on the catalytic activity were also discussed.

## 2. Experimental

### 2.1. Chemicals

Cobalt chloride hexahydrate (CoCl<sub>2</sub>·6H<sub>2</sub>O, Sinopharm Chemical Reagent Co. Ltd, > 99%), nickel chloride hexahydrate (NiCl<sub>2</sub>·6H<sub>2</sub>O, Sinopharm Chemical Reagent Co. Ltd, > 99%), aluminum chloride hexahydrate (AlCl<sub>3</sub>·6H<sub>2</sub>O, Sinopharm Chemical Reagent Co. Ltd, 99%), aluminum nitrate nonahydrate (Al(NO<sub>3</sub>)<sub>3</sub>·9H<sub>2</sub>O, Sinopharm Chemical Reagent Co. Ltd, 99%), chromium nitrate nonahydrate (Cr(NO<sub>3</sub>)<sub>3</sub>·9H<sub>2</sub>O, Sinopharm Chemical Reagent Co. Ltd, > 99%), potassium dichromate (K<sub>2</sub>Cr<sub>2</sub>O<sub>7</sub>, Sinopharm Chemical Reagent Co. Ltd, 99.8%), sodium hydroxide (NaOH, Sinopharm Chemical Reagent Co. Ltd, > 99%), 2-aminoterephthalic acid (C<sub>8</sub>H<sub>7</sub>NO<sub>4</sub>, Aldrich, 99%), terephthalic acid (C<sub>8</sub>H<sub>6</sub>O<sub>4</sub>, TA, Aldrich, 99%), N,N-dimethylformamide (DMF, Sinopharm Chemical Reagent Co. Ltd, 99.5%), sodium borohydride (NaBH<sub>4</sub>, J&K Chemical, 99%), ammonia borane (NH<sub>3</sub>BH<sub>3</sub>, Aldrich, 97%), nitric acid (HNO<sub>3</sub>, Beijing Chemical Plant, AR), sulfuric acid (H<sub>2</sub>SO<sub>4</sub>, Tianjin Chemical Reagent Factory, 95–98%), tin chloride dihydrate (SnCl<sub>2</sub>·2H<sub>2</sub>O, Sinopharm Chemical Reagent Co., Ltd., AR), 2-propanol ((CH<sub>3</sub>)<sub>2</sub>CHOH, Sinopharm Chemical Reagent Co. Ltd, 99.9%) and ethanol (CH<sub>3</sub>CH<sub>2</sub>OH, Sinopharm Chemical Reagent Co. Ltd, > 99%) were obtained without purification.

### 2.2. Synthesis and catalytic study

All the catalysts were synthesized using the impregnation and in-situ reduction processes. Typically, for the synthesis of Co/MIL-101(Cr)-NH<sub>2</sub>, the aqueous solution (2.0 mL) of MIL-101(Cr)-NH<sub>2</sub> (18 mg) and CoCl<sub>2</sub>·6H<sub>2</sub>O (0.034 mmol) was stirred in a two-necked flask for 5 h. The catalytic reaction began immediately under visible light irradiation at 298 K or in the dark at 298 K when the aqueous solution (1.5 mL) of NaBH<sub>4</sub> (0.068 mmol) and NH<sub>3</sub>BH<sub>3</sub> (1.71 mmol) was syringed into the above mixture. The molar ratio of metal/NH<sub>3</sub>BH<sub>3</sub> was kept as a constant of 0.02:1 in the catalytic processes. The cooling water

circulating pump was used to control the temperature of reaction solution at 298 K. The atmospheric pressure in Hohhot, Inner Mongolia was 88.8 kPa.

For comparison of the influences of different active metals and MOFs with different compositions and framework structures on the catalytic performance, other thirteen catalysts, Co/MIL-101(Al)-NH<sub>2</sub>, Co/MIL-53(Cr)-NH<sub>2</sub>, Co/MIL-53(Al)-NH<sub>2</sub>, Ni/MIL-101(Cr)-NH<sub>2</sub>, Ni/MIL-101(Al)-NH<sub>2</sub>, Ni/MIL-53(Cr)-NH<sub>2</sub>, Ni/MIL-53(Al)-NH<sub>2</sub>, Co/MIL-101(Cr), Co/MIL-53(Cr), Co/MIL-53(Al), Ni/MIL-101(Cr), Ni/MIL-53(Cr) and Ni/MIL-53(Al) were synthesized using the similar processes to those of Co/MIL-101(Cr)-NH<sub>2</sub>.

To test the stability of catalysts, 1.71 mmol of NH<sub>3</sub>BH<sub>3</sub> was added into the reaction flask under visible light irradiation after the previous H<sub>2</sub> evolution finished. Such cycle experiments were repeated for 25 times at 298 K. During the two adjacent catalytic cycles, the interval was 5 min.

### 2.3. Catalyst characterization

Powder X-ray diffraction (PXRD) measurements were performed on a Panalytical X-Pert X-ray diffractmeter. The transmission electron microscopy (TEM, JEM-2010) equipped with an energy dispersive X-ray (EDX) spectrometer was applied to confirm the morphologies and compositions of samples. The spectra of X-ray photoelectron spectroscopy (XPS) were acquired with an ESCALAB250 (Thermo VG Corp.). The UV-vis spectra were conducted on a spectrometer (Shimadzu UV-3600). The surface area measurements were performed using an automatic volumetric adsorption equipment (Autosorb-iQ2-MP). The IR spectra were recorded on a spectrometer (Thermo Fisher Scientific, NEXUS-670). The transient photocurrent measurements were carried out in an electrochemical station (PGSTAT302N, Switzerland). An indium tin oxide (ITO) glass plate coated with catalysts, a Pt plate and an Ag/AgCl electrode were used as the working electrode, the counter electrode and the reference electrode, respectively. The inductively coupled plasma-atomic emission spectroscopy (ICP-AES) measurement was performed on a Thermo Jarrell Ash (TJA) Atomscan Advantage instrument. The content measurement of C, H and N was carried out on a PerkinElmer 2400 instrument. The fluorescent spectra were obtained using a spectrometer (FLS920).

### 3. Calculation method

The TOF value was calculated from the following equation.

$$\text{TOF} = \frac{3n_{\text{NH}_3\text{BH}_3}}{n_{\text{metal}} t}$$

In the equation,  $n_{\text{metal}}$  is the total molar amount of metal species in the catalyst,  $t$  is reaction time, and  $n_{\text{NH}_3\text{BH}_3}$  is the total molar amount of NH<sub>3</sub>BH<sub>3</sub> in the catalytic reaction.

## 4. Results and discussion

### 4.1. Synthesis

Photoactive MOFs were selected to support non-noble metal NPs for catalyzing H<sub>2</sub> evolution from NH<sub>3</sub>BH<sub>3</sub> in aqueous solution under visible light irradiation since they can act as semiconductor-like species for harvesting visible light and producing hot electrons, which promote the catalytic reduction process. To achieve efficient semiconductor-like behaviors of photoactive MOFs, three ways can be adopted, namely, selecting electron-rich metal nodes, increasing the conjugation in the organic linkers and functionalizing the linkers with some groups such as NH<sub>2</sub> [49–53]. From the above considerations, four NH<sub>2</sub>-functionalized MOFs (MIL-101(Cr)-NH<sub>2</sub>, MIL-101(Al)-NH<sub>2</sub>, MIL-53(Cr)-NH<sub>2</sub> and MIL-53(Al)-NH<sub>2</sub>) were selected as photoactive supports. The NH<sub>2</sub> groups in these photoactive MOFs can immobilize metal NPs, resulting in the

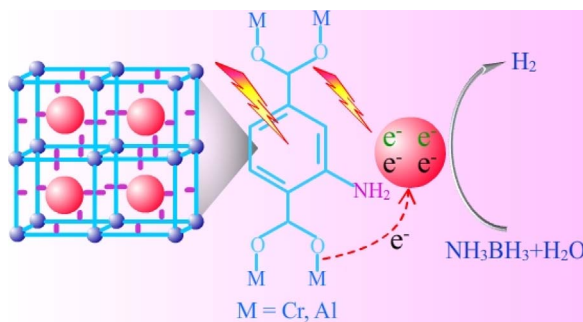


**Fig. 1.** Schematic illustration of the synergistic catalytic  $H_2$  evolution from  $NH_3BH_3$  in aqueous solution using non-plasmonic metal NPs supported by  $NH_2$ -functionalized photoactive MOFs under visible light irradiation.

effective electron transfer from photoactive MOFs to catalytically active metal NPs. In order to identify the contribution of these photoactive MOFs on catalytic activity, three  $NH_2$ -free MOFs (MIL-101(Cr), MIL-53(Cr) and MIL-53(Al)) were selected as non-photoactive supports to prepare supported metal catalysts. Moreover, the  $NH_2$  group in the photoactive MOFs has the interaction with  $BH_3$  group in catalytic substrate  $NH_3BH_3$ , leading to that the B–H bonds could be weakened and then the activation barrier of catalytic reaction could be reduced [22]. In a word, through the combination of these different  $NH_2$ -functionalized photoactive MOFs and non-plasmonic noble-metal-free NPs, which could generate hot electrons and excited electrons under visible light irradiation, respectively, the synergistic electron effect could lead to the remarkably tuned and enhanced activities of the supported catalysts in  $H_2$  evolution from aqueous  $NH_3BH_3$  solution, where there exists the splitting of B–N and B–H in  $NH_3BH_3$  and O–H in  $H_2O$  (Fig. 1).

#### 4.2. Characterization of the samples

TEM images of Co/MIL-101(Cr)-NH<sub>2</sub>, Co/MIL-101(Al)-NH<sub>2</sub>, Co/MIL-53(Cr)-NH<sub>2</sub>, Co/MIL-53(Al)-NH<sub>2</sub>, Ni/MIL-101(Cr)-NH<sub>2</sub> and Ni/MIL-101(Al)-NH<sub>2</sub> showed that Co and Ni NPs had different sizes and few aggregates (Fig. 2 and S1-4). From the selective area electron diffraction (SAED) patterns, it was found that the Co and Ni NPs in these catalysts were amorphous [14,69]. This was also verified by the PXRD patterns of these catalysts, where only the diffraction peaks of MOFs were observed and no apparent diffraction peaks of Co or Ni species were found (Fig. S5 and S6). These amorphous metal NPs might lead to the high catalytic activities since they have isotropic structures with much greater structural distortion and high concentrations of unsaturated coordination sites [70,71]. No observable contrast change was detected on the elemental maps recorded by the high angle annular dark field scanning TEM (HAADF-STEM) (Fig. 2 and S7), indicating the high dispersion of Co or Ni species in the catalysts. The EDX patterns further showed the presence of Co or Ni species in the catalysts (Fig. S8–13). From the PXRD patterns, it was also found the crystallinity of MOFs in the catalysts decreased due to that  $NaBH_4$  partially destroyed their porosity during the synthesis of catalysts [17]. The IR spectra of  $NH_2$ -functionalized MOFs and catalysts showed that the characteristic peaks of 2-aminoterephthalate linkers coordinated with metal ions in MOFs and corresponding catalysts after catalytic reaction were similar (Fig. 3). Especially, there were stretching vibration of N–H in the range of 3600–3300  $cm^{-1}$ , bending vibration of N–H in the range of 1600–1550  $cm^{-1}$  and stretching vibration of C–N in the range of 1300–1250  $cm^{-1}$ . In comparison with MOFs, the appreciable decrease in the surface areas of catalysts indicated that the pores of supports were occupied by metal NPs and/or blocked by metal NPs (Fig. S14) [72,73]. From the above results regarding PXRD, IR and  $N_2$  adsorption–desorption of MOFs and corresponding catalysts, it could be confirmed that the framework structures of MOFs were retained in the catalysts.

From the elemental analysis results, it was found the metal (Co or Ni) loading amounts were similar to the theoretical values and the organic ligands in MOFs existed in the catalysts (Table S1 and S2).

The XPS investigation showed that the peaks of Co 2p<sub>3/2</sub> and Co 2p<sub>1/2</sub> before Ar etching were observed with binding energies in the ranges of 781.0–781.9 and 796.9–797.9 eV corresponding to the Co 2p of CoO in the catalysts [14,69]. This was caused by the oxidation during the exposure of catalysts in the air (Fig. S15–18). However, the peaks in the ranges of 778.1–778.9 and 793.0–793.9 eV of metallic Co species were detected after Ar etching, indicating that metallic Co species were active components for the in-situ catalytic  $H_2$  evolution. In addition, Ni species in the catalysts also exhibited the similar phenomenon (Fig. S19 and S20). In comparison with the binding energy of N in the  $NH_2$ -functionalized supports, the binding energy of N in the catalysts containing these supports slightly increased (Fig. S21–23), indicating that there existed the interactions between metal NPs and the  $NH_2$  groups in MOFs. It should be noted that compared with the binding energy of O in the  $NH_2$ -functionalized and  $NH_2$ -free supports, the binding energy of O in all the catalysts slightly decreased (Fig. S24–28). This indicated that the change of binding energy of O in the MOF-supported metal catalysts was not caused by the functional  $NH_2$  groups but caused by the presence of metal NPs. Since the UV-vis absorption behavior is associated with the photoinduced electron transfer process of a photocatalyst, the UV-vis spectra of photoactive MOFs and catalysts were measured. The results showed that there were intensive absorption peaks ranging from 300 to 450 nm, which were associated with the chromophore in the 2-aminoterephthalate linker of MOFs. Also, the presence of metal NPs did not significantly affect the optical properties of MOFs in the catalysts (Fig. 4). Other adsorptions were caused by that the bound electrons of Co or Ni species in the catalysts excited individual electrons to the high energy levels [49–53].

#### 4.3. Catalytic performance

In order to explore the effect of visible light, which is an ideal power source to drive chemical reactions, on the catalytic performance, the catalytic  $H_2$  evolution from  $NH_3BH_3$  over the four catalysts Co/MIL-101(Cr)-NH<sub>2</sub>, Co/MIL-101(Al)-NH<sub>2</sub>, Co/MIL-53(Cr)-NH<sub>2</sub> and Co/MIL-53(Al)-NH<sub>2</sub> was tested under visible light irradiation and in the dark. As shown in Fig. 5, compared with the activities of the catalysts in the dark, their activities were significantly enhanced under visible light irradiation. Among the four catalysts, Co/MIL-101(Cr)-NH<sub>2</sub> exhibited the highest activity with the total TOF value of 117.7  $min^{-1}$ , which was the highest in the values of all the reported non-noble metal catalysts and were even comparable to the values of noble metal catalysts at 298 K (Table 1). It should be noted that other three catalysts Co/MIL-101(Al)-NH<sub>2</sub>, Co/MIL-53(Cr)-NH<sub>2</sub> and Co/MIL-53(Al)-NH<sub>2</sub> also had the higher activities than all the reported non-noble metal catalysts. Moreover, the activity enhancement of 161.5, 126.4, 132.4 and 127.6% was resulted from the contribution of visible light irradiation using Co/MIL-101(Cr)-NH<sub>2</sub>, Co/MIL-101(Al)-NH<sub>2</sub>, Co/MIL-53(Cr)-NH<sub>2</sub> and Co/MIL-53(Al)-NH<sub>2</sub> compared with the dark reaction, respectively. The difference in the increased activity could be ascribed to the different visible light absorption ability of  $NH_2$ -functionalized MOFs with different compositions and framework structures, which might lead to the different amounts of photogenerated electrons transferred from MOFs to active metal NPs. In addition, four pure photoactive MOFs, MIL-101(Cr)-NH<sub>2</sub>, MIL-101(Al)-NH<sub>2</sub>, MIL-53(Cr)-NH<sub>2</sub> and MIL-53(Al)-NH<sub>2</sub>, had no catalytic activities, further confirming that metal NPs were the catalytically active species for  $H_2$  evolution from  $NH_3BH_3$  (Fig. S29 and S30). It should be noted that  $H_2O$  might play the role of sacrificial reagent to capture the photogenerated holes [17], resulting in the formation of hydroxyl radicals and efficient separation of electrons and holes generated from semiconductor-like MOFs under visible light irradiation. In order to explore the influence of hydroxyl radicals on the catalytic activity, we used TA as fluorescence probe to detect the

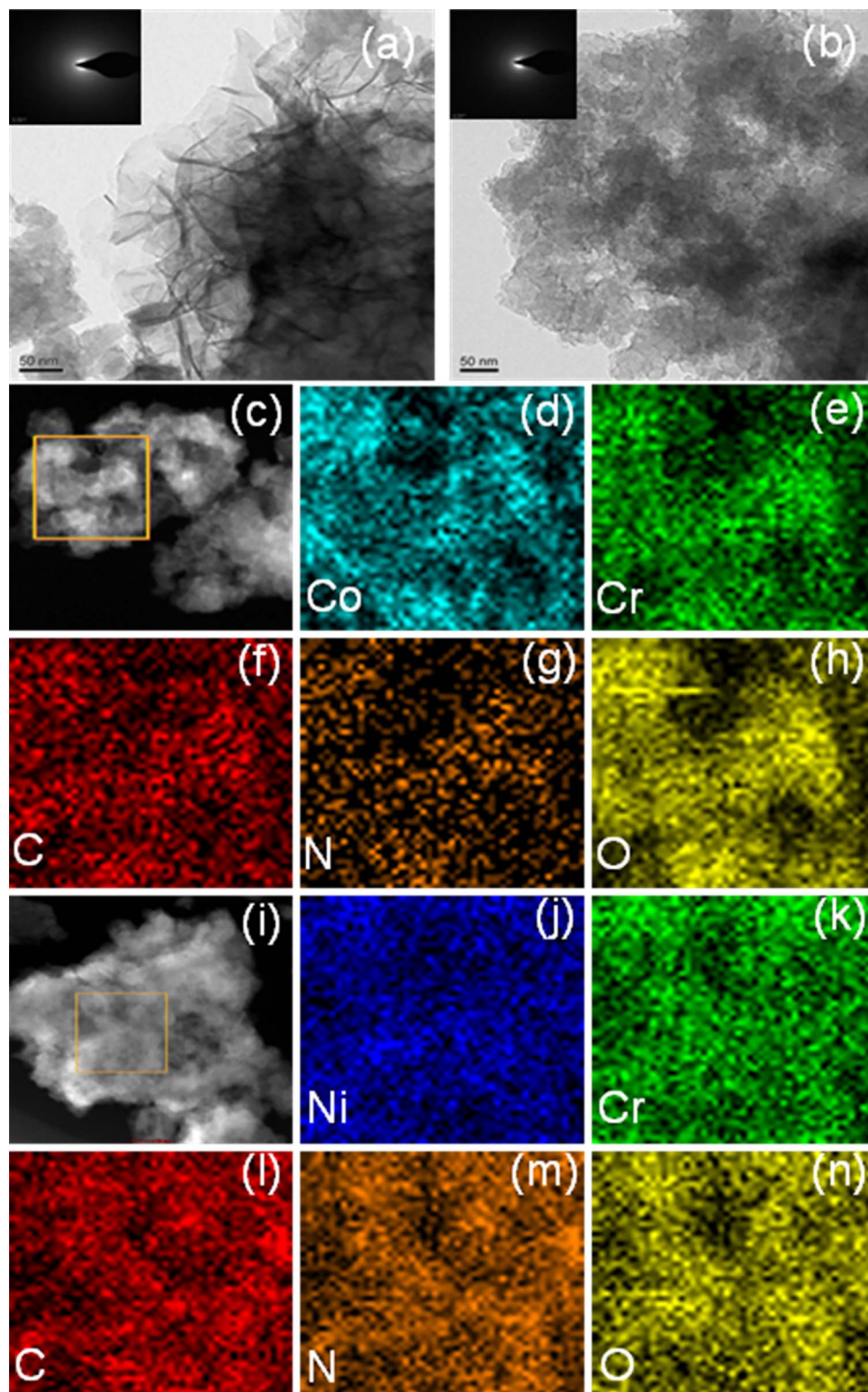
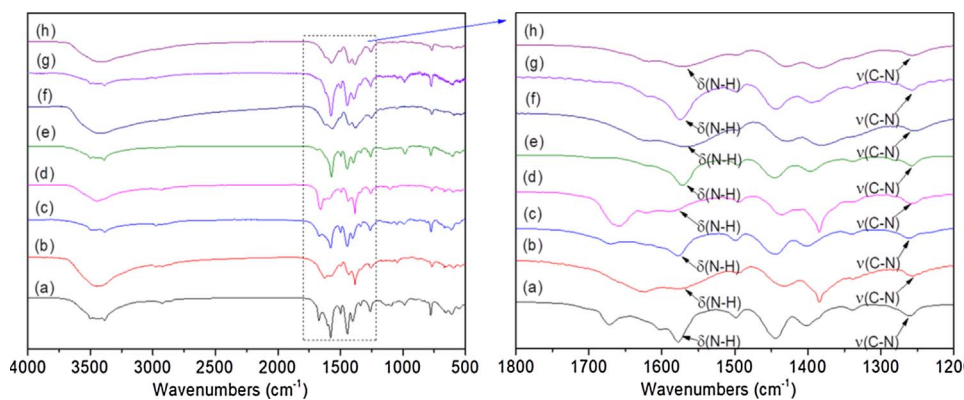


Fig. 2. TEM images, SAED patterns (insets) and HAADF-STEM images of (a, c) Co/MIL-101(Cr)-NH<sub>2</sub> and (b, i) Ni/MIL-101(Cr)-NH<sub>2</sub> and the corresponding elemental maps of Co/MIL-101(Cr)-NH<sub>2</sub> for (d) Co, (e) Cr, (f) C, (g) N and (h) O and Ni/MIL-101(Cr)-NH<sub>2</sub> for (j) Ni, (k) Cr, (l) C, (m) N and (n) O.

radicals under visible light irradiation. The results showed that there were no fluorescence peaks in the absence of Co/MIL-101(Cr)-NH<sub>2</sub> and the fluorescence peak of Co/MIL-101(Cr)-NH<sub>2</sub> appeared at 426 nm in the absence of TA (Fig. 6). This fluorescence peak might be produced by the reaction between the organic linkers of MIL-101(Cr)-NH<sub>2</sub> and photogenerated hydroxyl radicals. After introducing TA, the fluorescence peak was significantly enhanced, indicating that the high concentration of hydroxyl radicals could form in the presence of Co/MIL-

101(Cr)-NH<sub>2</sub> under visible light irradiation. A similar intensive fluorescence peak was observed after introducing NH<sub>3</sub>BH<sub>3</sub> in the above solution. Moreover, the catalytic activity of Co/MIL-101(Cr)-NH<sub>2</sub> decreased after introducing TA (12.0 mM) (Fig. 7), suggesting that the hydroxyl radicals indeed played an important role in enhancing the photocatalytic activity. In order to further confirm the existence of hydroxyl radicals in the present photocatalytic system, we also measured the photocatalytic activity of Co/MIL-101(Cr)-NH<sub>2</sub>, where 2-



**Fig. 3.** IR spectra of  $\text{NH}_2$ -functionalized photoactive MOFs and the corresponding supported catalysts: (a) MIL-53(Al)- $\text{NH}_2$ , (b) MIL-53(Cr)- $\text{NH}_2$ , (c) MIL-101(Al)- $\text{NH}_2$ , (d) MIL-101(Cr)- $\text{NH}_2$ , (e) Co/MIL-53(Al)- $\text{NH}_2$ , (f) Co/MIL-53(Cr)- $\text{NH}_2$ , (g) Co/MIL-101(Al)- $\text{NH}_2$ , (h) Co/MIL-101(Cr)- $\text{NH}_2$ .

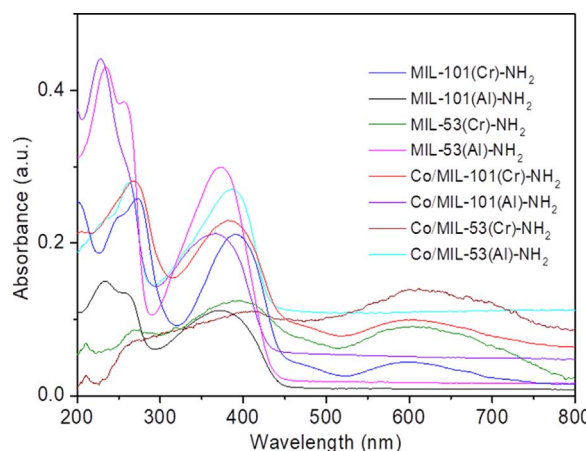


**Fig. 4.** UV-vis spectra of  $\text{NH}_2$ -functionalized photoactive MOFs and the corresponding supported catalysts.

propanol was used as capture agent of hydroxyl radicals. The results showed that compared with the photocatalytic activity without 2-propanol, its activity significantly decreased in the presence of 2-propanol (90  $\mu\text{L}$ ) (Fig. 7).

The generality of the catalytic method is important. To check this generality, we studied the catalytic performance of the four Ni-based catalysts Ni/MIL-101(Cr)- $\text{NH}_2$ , Ni/MIL-101(Al)- $\text{NH}_2$ , Ni/MIL-53(Cr)- $\text{NH}_2$  and Ni/MIL-53(Al)- $\text{NH}_2$  under visible light irradiation and in the dark. The results showed that their catalytic orderliness was similar to that in the Co-based catalysts (Fig. 8). The visible light irradiation led to the activity enhancement of Ni/MIL-101(Cr)- $\text{NH}_2$ , Ni/MIL-101(Al)- $\text{NH}_2$ , Ni/MIL-53(Cr)- $\text{NH}_2$  and Ni/MIL-53(Al)- $\text{NH}_2$  was 122.0, 141.2, 226.8 and 238.9%, respectively.

To confirm the contribution of semiconductor-like characteristics of MOFs on the enhanced  $\text{H}_2$  evolution, three  $\text{NH}_2$ -free non-photoactive MOFs (MIL-101(Cr), MIL-53(Cr) and MIL-53(Al)) were selected as supports to prepare six Co and Ni catalysts. The PXRD and IR investigations showed that the framework structures of these non-photoactive MOFs were kept in the catalysts (Fig. S31–34). Co/MIL-101(Cr) was selected as an example to explore the microstructure of Co NPs. The results showed that the amorphous Co NPs were dispersed on MIL-101(Cr), which was testified by the TEM, HAADF-STEM, SAED and EDX characterizations (Fig. S35 and S36). The catalytic results also showed that there was activity enhancement of the six catalysts under visible light irradiation (Fig. 9 and S37). The activity enhancement of 51.1, 74.4, 113.5, 106.6, 105.9 and 92.9% was resulted from the contribution of visible light irradiation using Co/MIL-101(Cr), Co/MIL-53(Cr), Co/MIL-53(Al), Ni/MIL-101(Cr), Ni/MIL-53(Cr) and Ni/MIL-53(Al) compared with the dark reaction, respectively. The enhanced activity was mainly due to that the visible light irradiation induced the interband

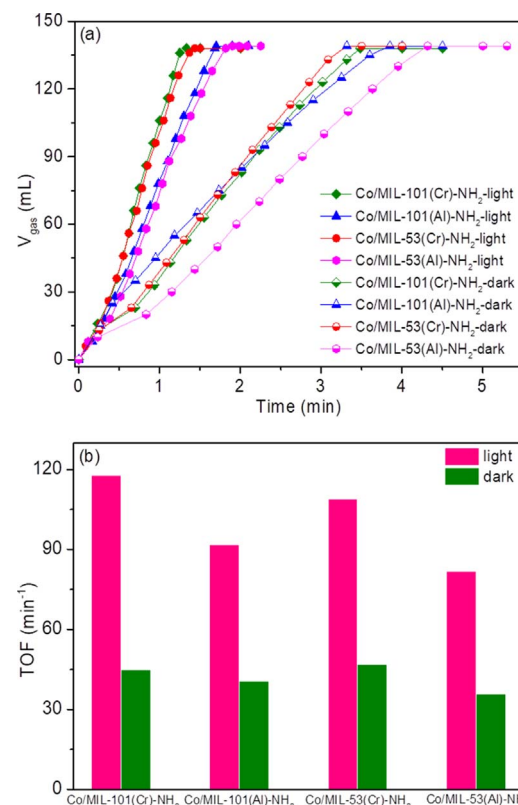


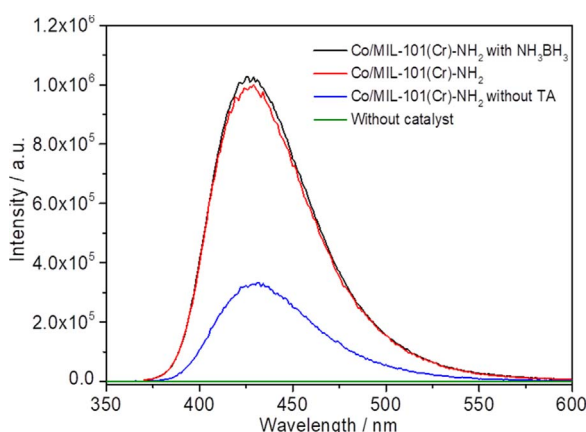
**Fig. 5.** (a) Plots of time versus volume of  $\text{H}_2$  evolution from  $\text{NH}_3\text{BH}_3$  aqueous solution over Co NPs supported by  $\text{NH}_2$ -functionalized photoactive MOFs under visible light irradiation and in the dark and (b) the total TOF values of the catalysts.

electron transition of non-plasmonic Co and Ni NPs and thus led to the generation of excited electrons, which in turn enriched their electron density.

In order to explore the electronic characteristics of catalysts, we have measured the transient photocurrent density of Co/MIL-101(Cr)- $\text{NH}_2$  and Co/MIL-101(Cr) as examples under visible light irradiation ( $> 420 \text{ nm}$ ). The results clearly showed that the photocurrent generated in both catalysts, but the photocurrent of Co/MIL-101(Cr)- $\text{NH}_2$  was much higher than that of Co/MIL-101(Cr) (Fig. 10), which strongly illustrated that the migration efficiency of photoinduced charge carriers was promoted in Co/MIL-101(Cr)- $\text{NH}_2$ . This result also indicated that the electron density of Co NPs in Co/MIL-101(Cr)- $\text{NH}_2$  was remarkably enhanced through the synergistic electron contribution of themselves and photoactive MIL-101(Cr)- $\text{NH}_2$ , resulting in the remarkably enhanced photocatalytic activity. In order to verify the electron contribution of non-plasmonic Co and Ni NPs to the catalysis, we systematically studied the transient photocurrent density of the six catalysts

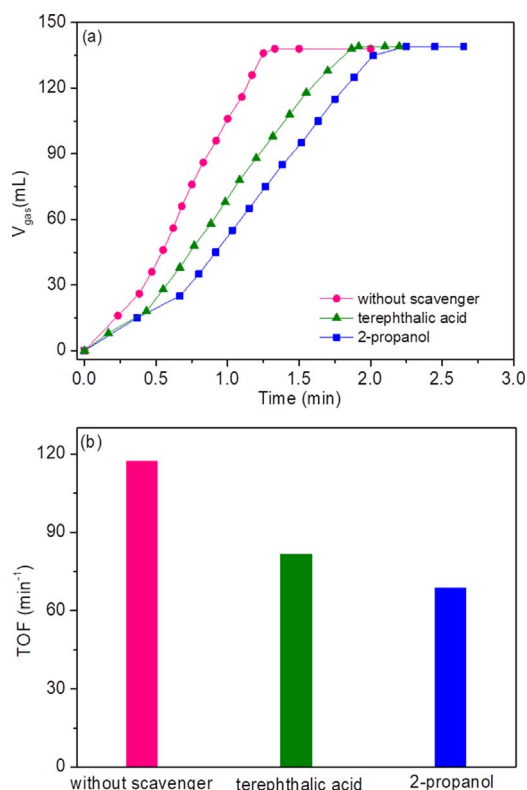
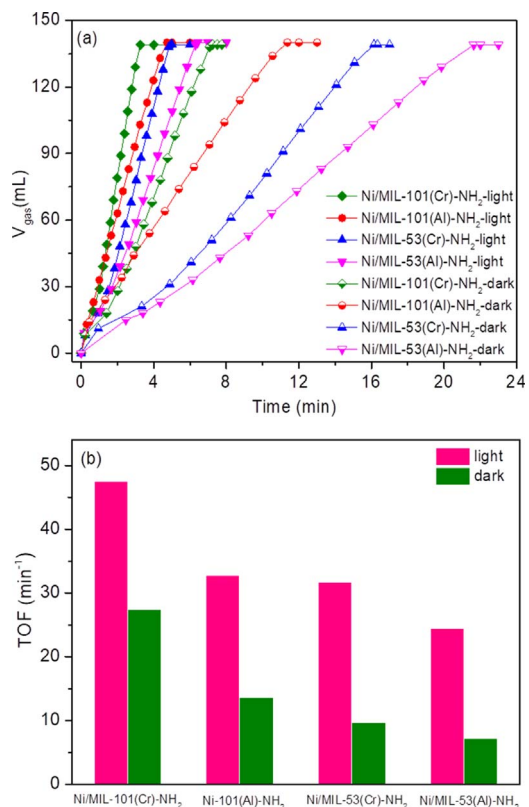
**Table 1**Activities of catalysts in the  $H_2$  evolution from  $NH_3BH_3$  at 298 K.

Catalyst	TOF (min <sup>-1</sup> )	Reference
Co/MIL-101(Cr)-NH <sub>2</sub>	117.7	This work
Co/MIL-53(Cr)-NH <sub>2</sub>	108.9	This work
Co/MIL-101(Al)-NH <sub>2</sub>	91.9	This work
Co/MIL-53(Al)-NH <sub>2</sub>	81.7	This work
PdCo/C	35.7	8
Ru@HAP	137	10
PtRu alloys	90	15
AuNi@MIL-101	66.2	11
AuCo/NCX-1	42.1	14
Co nanoparticles	39.8	20
Cu@Co	15	21
CuNi/graphene	16.4	23
CuNi/MCNS	54.8	26
Ni <sub>2</sub> P	40.4	27
CuCo/C	45	29
Cu <sub>0.8</sub> Co <sub>0.2</sub> O-GO	70	30
Co/CTF-1	42.3	31
Co/g-C <sub>3</sub> N <sub>4</sub> -1	55.6	43

**Fig. 6.** Fluorescent spectra of the samples in the aqueous solution containing NaOH (4.0 mM) and TA (5.0 mM) at different conditions under visible light irradiation for 5 mins.

based on NH<sub>2</sub>-free MOFs. The results showed that the low transient photocurrent appeared in all the six catalysts under visible light irradiation (Fig. S38 and S39). The generated photocurrent could be originated from the interband electron transitions of non-plasmonic metal NPs [45,46].

To further understand the enhancement of the photocatalytic activities of catalysts, the dependence of light intensity on the catalytic  $H_2$  evolution using Co/MIL-101(Cr)-NH<sub>2</sub>, Co/MIL-53(Al)-NH<sub>2</sub>, Ni/MIL-101(Cr)-NH<sub>2</sub> and Ni/MIL-53(Al)-NH<sub>2</sub> were investigated. The results showed that increasing the light intensity led to an almost linear increase in the  $H_2$  evolution rate of  $NH_3BH_3$  (Fig. 11 and S40-42). The above phenomena could be ascribed to that more photogenerated electrons were motivated from photoactive MOFs and non-plasmonic Co (Ni) NPs under the light irradiation with high intensity, resulting in the enhanced electron density of supported Co (Ni) NPs and the resultant enhanced catalytic activities. In order to clarify the effect of electrons on the photocatalytic hydrogen generation from  $NH_3BH_3$ , we selected K<sub>2</sub>Cr<sub>2</sub>O<sub>7</sub> as the electron capture to measure the activities of Co/MIL-101(Cr)-NH<sub>2</sub>, Co/MIL-101(Al)-NH<sub>2</sub>, Co/MIL-53(Cr)-NH<sub>2</sub> and Co/MIL-53(Al)-NH<sub>2</sub> under visible light irradiation. The results showed that compared with the photocatalytic activity of the four catalysts without K<sub>2</sub>Cr<sub>2</sub>O<sub>7</sub>, their activity significantly decreased in the presence of K<sub>2</sub>Cr<sub>2</sub>O<sub>7</sub> (100  $\mu$ M) (Fig. S43-46). This indicated that the amounts of photogenerated electrons decreased due to that the dichromate efficiently captured the photogenerated electrons from the semiconducting

**Fig. 7.** (a) Plots of time versus volume of  $H_2$  evolution from  $NH_3BH_3$  aqueous solution over Co/MIL-101(Cr)-NH<sub>2</sub> in the presence or absence of TA and 2-propanol under visible light irradiation and (b) the corresponding total TOF values of the catalyst.**Fig. 8.** (a) Plots of time versus volume of  $H_2$  evolution from  $NH_3BH_3$  aqueous solution over Ni NPs supported by NH<sub>2</sub>-functionalized photoactive MOFs under visible light irradiation and in the dark and (b) the total TOF values of the catalysts.

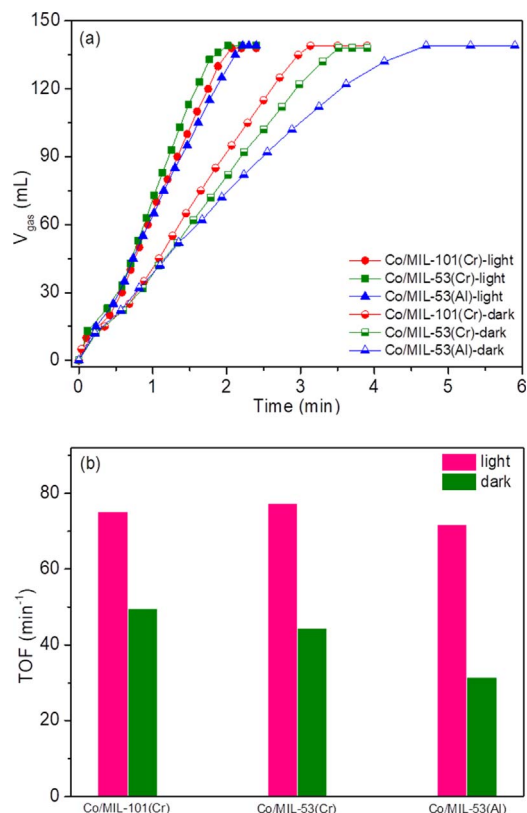


Fig. 9. (a) Plots of time versus volume of  $\text{H}_2$  evolution from  $\text{NH}_3\text{BH}_3$  aqueous solution over Co NPs supported by  $\text{NH}_2$ -free non-photoactive MOFs under visible light irradiation and in the dark and (b) the total TOF values of the catalysts.

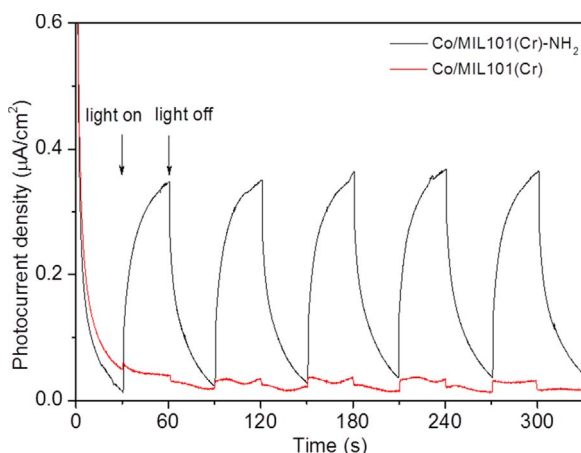


Fig. 10. Profiles of time versus transient photocurrent density of two different Co catalysts.

catalysts under visible light irradiation [74,75].

In many cases, the reaction temperature influences the photocatalytic performance of a catalyst [46,48]. So the photocatalytic activity of Co/MIL-101(Cr)-NH<sub>2</sub> was measured under the different temperatures (313 and 333 K). The results showed that compared with the activity of Co/MIL-101(Cr)-NH<sub>2</sub> at 298 K, its activity was significantly enhanced under photothermal conditions (Fig. S47). The TOF values of Co/MIL-101(Cr)-NH<sub>2</sub> at 313 and 333 K were 208.8 and 412.2  $\text{min}^{-1}$ , respectively, which were much higher than its room-temperature TOF value (117.7  $\text{min}^{-1}$ ).

The recycle durability is of importance in the practical application of catalysts. So the photocatalytic long-time durability tests of Co/MIL-101(Cr)-NH<sub>2</sub>, Ni/MIL-101(Cr)-NH<sub>2</sub> and Co/MIL-53(Al)-NH<sub>2</sub> were

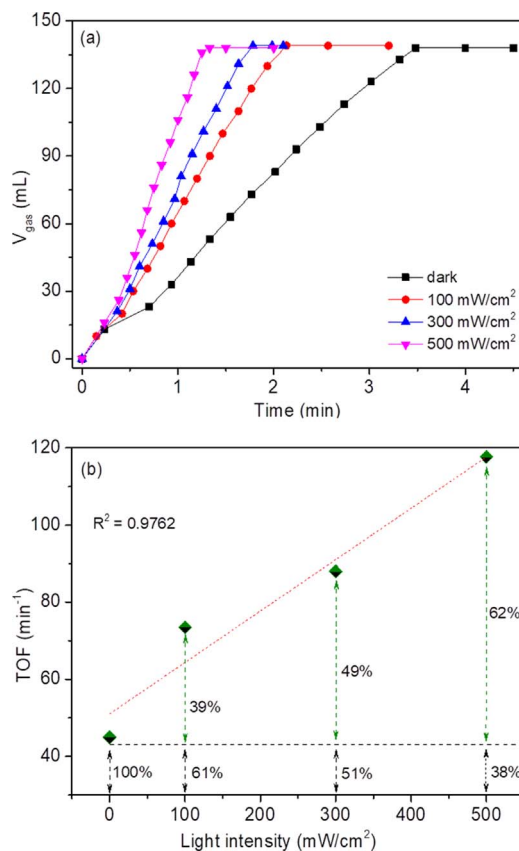


Fig. 11. (a) Plots of time versus volume of  $\text{H}_2$  evolution from  $\text{NH}_3\text{BH}_3$  aqueous solution over Co/MIL-101(Cr)-NH<sub>2</sub> under visible light irradiation with different intensities and (b) the dependence of total TOF values on the light intensity.

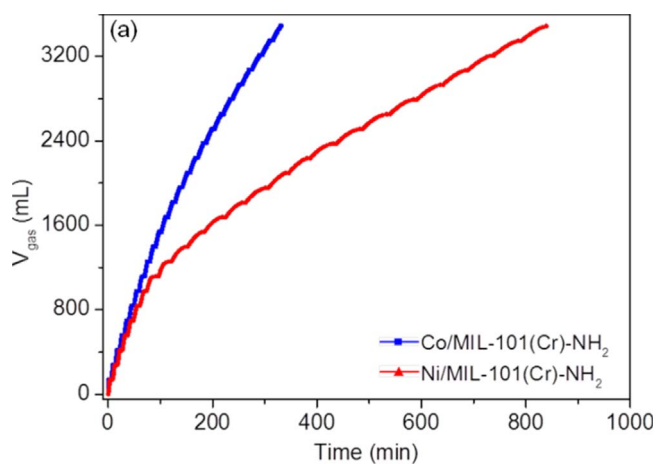


Fig. 12. (a) Long-time photocatalytic durability test for the  $\text{H}_2$  evolution from  $\text{NH}_3\text{BH}_3$  aqueous solution over two catalysts and the TEM images and SAED patterns (insets) of (b) Co/MIL-101(Cr)-NH<sub>2</sub> and (c) Ni/MIL-101(Cr)-NH<sub>2</sub> after 25 runs of catalysis.

carried out at 298 K. As shown in Fig. 12a and S48, even after 25 runs, the productivity of H<sub>2</sub> remained unchanged and their activities had no significant change; the durability of Co/MIL-101(Cr)-NH<sub>2</sub> and Co/MIL-53(Al)-NH<sub>2</sub> was higher than that of Ni/MIL-101(Cr)-NH<sub>2</sub>, which was probably due to the relatively large agglomeration of Ni NPs after the long-time photocatalytic process (Fig. 12b, 12c, S49, S50 and S51). Moreover, the catalytically active sites could be blocked by boron species, always leading to the activity decrease during the long-time catalytic reaction [7–31]. The PXRD and IR results of the three catalysts showed the framework structures of MIL-101(Cr)-NH<sub>2</sub> and MIL-53(Al)-NH<sub>2</sub> were not significantly changed after the 25 runs of catalytic hydrogen evolution (Fig. S52 and S53).

## 5. Conclusions

In summary, a series of non-plasmonic Co and Ni NPs supported by seven photoactive and non-photoactive MOFs were designed and synthesized, which exhibited the enhanced catalytic activities in H<sub>2</sub> evolution from NH<sub>3</sub>BH<sub>3</sub> under visible light irradiation. Among all the catalysts, the Co-based catalysts based on photoactive MOFs with hydrophilicity had the highest activities among the reported noble-metal-free catalysts at 298 K. The synergistic electron effect of NH<sub>2</sub>-functionalized photoactive MOFs and non-plasmonic metal NPs ensured the remarkably enhanced activities. Moreover, the incident light intensity-dependent catalytic activity enhancement verified that the visible light irradiation indeed led to the enrichment of electron density of Co and Ni NPs in the light-responsive catalysts. Through exploring the synergistic electron effect of non-plasmonic metal NPs and semiconductor-like photoactive MOFs, which have tunable well-defined structures and different visible light absorption characteristics, to tailor the electron behaviors of catalytically active metal centers, it is possible to design novel photocatalytic systems using noble-metal-free nanomaterials as high-performance catalysts toward a greener world.

## Acknowledgements

The authors gratefully acknowledge the financial support from the Program for New Century Excellent Talents in University of the Ministry of Education of China (grant no. NCET-13-0846) and the Program for Young Talents of Science and Technology in Universities of Inner Mongolia Autonomous Region (grant no. NJYT-13-A01).

## Appendix A. Supplementary data

Supplementary data associated with this article can be found, in the online version, at <https://doi.org/10.1016/j.apcatb.2017.12.024>.

## References

- A. Staibitz, A.P.M. Robertson, I. Manners, *Chem. Rev.* 110 (2010) 4079–4124.
- X. Gu, Z.-H. Lu, H.-L. Jiang, T. Akita, Q. Xu, *J. Am. Chem. Soc.* 133 (2011) 11822–11825.
- A. Boddien, D. Mellmann, F. Gärtner, R. Jackstell, H. Junge, P.J. Dyson, G. Laurenczy, R. Ludwig, M. Beller, *Science* 333 (2011) 1733–1736.
- A. Gutowski, L. Li, Y. Shin, C.M. Wang, X.S. Li, J.C. Linehan, R.S. Smith, B.D. Kay, B. Schmid, W. Shaw, M. Gutowski, T. Autrey, *Angew. Chem. Int. Ed.* 44 (2005) 3578–3582.
- Z. Xiong, C.K. Yong, G.T. Wu, P. Chen, W. Shaw, A. Karkamkar, T. Autrey, M.O. Jones, S.R. Johnson, P.P. Edwards, W.I.F. David, *Nat. Mater.* 7 (2008) 138–141.
- Z. Tang, H. Chen, X. Chen, L. Wu, X. Yu, *J. Am. Chem. Soc.* 134 (2012) 5464–5467.
- M. Chandra, Q. Xu, *J. Power Sources* 168 (2007) 135–142.
- D. Sun, V. Mazumder, Ö. Metin, S. Sun, *ACS Nano* 5 (2011) 6458–6464.
- J. Wang, Y.-L. Qin, X. Liu, X.-B. Zhang, *J. Mater. Chem.* 22 (2012) 12468–12470.
- S. Akbayrak, P. Erdek, S. Özkar, *Appl. Catal. B: Environ.* 142–143 (2013) 187–195.
- Q.-L. Zhu, J. Li, Q. Xu, *J. Am. Chem. Soc.* 135 (2013) 10210–10213.
- Q. Yao, W. Shi, G. Feng, Z.-H. Lu, X. Zhang, D. Tao, D. Kong, X. Chen, *J. Power Sources* 257 (2014) 293–299.
- Y.-Z. Chen, Q. Xu, S.-H. Yu, H.-L. Jiang, *Small* 11 (2015) 71–76.
- L. Guo, X. Gu, K. Kang, Y. Wu, J. Cheng, P. Liu, T. Wang, H. Su, *J. Mater. Chem. A* 3 (2015) 22807–22815.
- Q. Zhu, C. Xu, *Chem. Asian J.* 11 (2016) 705–712.
- M. Rakap, *Appl. Catal. B: Environ.* 163 (2015) 129–134.
- M. Wen, Y. Cui, Y. Kuwahara, K. Mori, H. Yamashita, *ACS Appl. Mater. Interfaces* 8 (2016) 21278–21284.
- H. Ye, Q. Wang, M. Catalano, N. Lu, J. Vermeylen, M.J. Kim, Y. Liu, Y. Sun, X. Xia, *Nano Lett.* 16 (2016) 2812–2817.
- W.-W. Zhang, Q.-L. Zhu, Q. Xu, *ACS Catal.* 6 (2016) 6892–6905.
- J.-M. Yan, X.-B. Zhang, H. Shioyama, Q. Xu, *J. Power Sources* 195 (2010) 1091–1094.
- H.-L. Jiang, Q. Xu, *Chem. Commun.* 47 (2011) 3351–3370.
- J. Hu, Z. Chen, M. Li, X. Zhou, H. Lu, *ACS Appl. Mater. Interfaces* 6 (2014) 13191–13200.
- W. Feng, L. Yang, N. Cao, C. Du, H. Dai, W. Luo, G. Cheng, *Int. J. Hydrogen Energy* 39 (2014) 3371–3380.
- F. Qiu, Y. Dai, L. Li, C. Xu, Y. Huang, C. Chen, Y. Wang, L. Jiao, H. Yuan, *Int. J. Hydrogen Energy* 39 (2014) 436–441.
- D. Özhan, N.Z. Külcüşlan, S. Özkar, *Appl. Catal. B: Environ.* 162 (2015) 573–582.
- H. Yen, Y. Seo, S. Kaliaguine, F. Kleitz, *ACS Catal.* 5 (2015) 5505–5511.
- C.-Y. Peng, L. Kang, S. Cao, Y. Chen, Z.-S. Lin, W.-F. Fu, *Angew. Chem. Int. Ed.* 54 (2015) 15725–15729.
- Q. Yao, Z.-H. Lu, W. Huang, X. Chen, J. Zhu, *J. Mater. Chem. A* 4 (2016) 8579–8583.
- A. Bulut, M. Yurderi, E. i. Ertas, M. Celebi, M. Kaya, M. Zahmakiran, *Appl. Catal. B: Environ.* 180 (2016) 121–129.
- K. Feng, J. Zhong, B. Zhao, H. Zhang, L. Xu, X. Sun, S.-T. Lee, *Angew. Chem. Int. Ed.* 55 (2016) 11950–11954.
- Z. Li, T. He, L. Liu, W. Chen, M. Zhang, G. Wu, P. Chen, *Chem. Sci.* 8 (2017) 781–788.
- W. Zhu, R. Michalsky, Ö. Metin, H. Lv, S. Guo, C.J. Wright, X. Sun, A.A. Peterson, S. Sun, *J. Am. Chem. Soc.* 135 (2013) 16833–16836.
- Z. Zhao, J. Arentz, L.A. Pretzer, P. Limpornpipat, J.M. Clomburg, R. Gonzalez, N.M. Schweitzer, T. Wu, J.T. Miller, M.S. Wong, *Chem. Sci.* 5 (2014) 3715–3728.
- J. Cheng, X. Gu, X. Sheng, P. Liu, H. Su, *J. Mater. Chem. A* 4 (2016) 1887–1894.
- H. Tsunoyama, N. Ichikuni, H. Sakurai, T. Tsukuda, *J. Am. Chem. Soc.* 131 (2009) 7086–7093.
- S. Jones, J. Qu, K. Tedesree, X.-Q. Gong, S.C.E. Tsang, *Angew. Chem. Int. Ed.* 51 (2012) 11275–11278.
- D. Wang, Y. Li, *Adv. Mater.* 23 (2011) 1044–1060.
- J. Liu, N.P. Wichramaratne, S.Z. Qiao, M. Jaroniec, *Nat. Mater.* 14 (2015) 763–774.
- M. Yoshida, A. Yamakata, K. Takanabe, J. Kubota, M. Osawa, K. Domen, *J. Am. Chem. Soc.* 131 (2009) 13218–13219.
- T. Kamegawa, S. Matsuura, H. Seto, H. Yamashita, *Angew. Chem. Int. Ed.* 52 (2013) 916–919.
- Y. Ma, X. Wang, Y. Jia, X. Chen, H. Han, C. Li, *Chem. Rev.* 114 (2014) 9987–10043.
- L.-T. Guo, Y.-Y. Cai, J.-M. Ge, Y.-N. Zhang, L.-H. Gong, X.-H. Li, K.-X. Wang, Q.-Z. Ren, J. Sun, J.-S. Chen, *ACS Catal.* 5 (2015) 388–392.
- H. Zhang, X. Gu, P. Liu, J. Song, J. Cheng, H. Su, *J. Mater. Chem. A* 5 (2017) 2288–2296.
- F. Sastre, A.V. Puga, L. Liu, A. Corma, H. García, *J. Am. Chem. Soc.* 136 (2014) 6798–6801.
- S. Sarina, H.-Y. Zhu, Q. Xiao, E. Jaatinen, J. Jia, Y. Huang, Z. Zheng, H. Wu, *Angew. Chem. Int. Ed.* 53 (2014) 2935–2940.
- X. Meng, T. Wang, L. Liu, S. Ouyang, P. Li, H. Hu, T. Kako, H. Iwai, A. Tanaka, J. Ye, *Angew. Chem. Int. Ed.* 53 (2014) 11478–11482.
- X.-N. Guo, Z.-F. Jiao, G.-Q. Jin, X.-Y. Guo, *ACS Catal.* 5 (2015) 3836–3840.
- Y. Zhao, B. Zhao, J. Liu, G. Chen, R. Gao, S. Yao, M. Li, Q. Zhang, L. Gu, J. Xie, X. Wen, L.-Z. Wu, C.-H. Tung, D. Ma, T. Zhang, *Angew. Chem. Int. Ed.* 55 (2016) 4215–4219.
- T. Zhang, W. Lin, *Chem. Soc. Rev.* 43 (2014) 5982–5993.
- S. Wang, X. Wang, *Small* 11 (2015) 3097–3112.
- A. Dhakshinamoorthy, A.M. Asiri, H. García, *Angew. Chem. Int. Ed.* 55 (2016) 5414–5445.
- L. Zeng, X. Guo, C. He, C. Duan, *ACS Catal.* 6 (2016) 7935–7947.
- M. Wen, K. Mori, Y. Kuwahara, T. An, H. Yamashita, *Appl. Catal. B: Environ.* 218 (2017) 555–569.
- X. Hao, Z. Jin, H. Yang, G. Lu, Y. Bi, *Appl. Catal. B: Environ.* 210 (2017) 45–56.
- Y. Fu, D. Sun, Y. Chen, R. Huang, Z. Ding, X. Fu, Z. Li, *Angew. Chem. Int. Ed.* 51 (2012) 3364–3367.
- K.G.M. Laurier, F. Vermoortele, R. Ameloot, D.E. De Vos, J. Hofkens, M.B.J. Roeaers, *J. Am. Chem. Soc.* 135 (2013) 14488–14491.
- L. Shen, M. Luo, Y. Liu, R. Liang, F. Jing, L. Wu, *Appl. Catal. B: Environ.* 166–167 (2015) 445–453.
- X.-Y. Dong, M. Zhang, R.-B. Pei, Q. Wang, D.-H. Wei, S.-Q. Zang, Y.-T. Fan, T.C.W. Mak, *Angew. Chem. Int. Ed.* 55 (2016) 2073–2077.
- J.-X. Liu, M.-Y. Gao, W.-H. Fang, L. Zhang, J. Zhang, *Angew. Chem. Int. Ed.* 55 (2016) 5160–5165.
- D. Kim, D.R. Whang, S.Y. Park, *J. Am. Chem. Soc.* 138 (2016) 8698–8701.
- Y. Gao, S. Li, Y. Li, L. Yao, H. Zhang, *Appl. Catal. B: Environ.* 202 (2017) 165–174.
- Y.-Z. Chen, Z.U. Wang, H. Wang, J. Lu, S.-H. Yu, H.-L. Jiang, *J. Am. Chem. Soc.* 139 (2017) 2035–2044.
- S. Kitagawa, R. Kitaura, S.-i. Noro, *Angew. Chem. Int. Ed.* 43 (2004) 2334–2375.
- M. O'Keeffe, O.M. Yaghi, *Chem. Rev.* 112 (2012) 675–702.
- L.E. Kreno, K. Leong, O.K. Farha, M. Allendorf, R.P. Van Duyne, J.T. Hupp, *Chem. Rev.* 112 (2012) 1105–1125.
- M. Eddaoudi, D.F. Sava, J.F. Eubank, K. Adil, V. Guillerm, *Chem. Soc. Rev.* 44 (2015) 228–249.

[67] X. Li, T.W. Goh, L. Li, C. Xiao, Z. Guo, X.C. Zeng, W. Huang, *ACS Catal.* 6 (2016) 3461–3468.

[68] J. Cheng, X. Gu, P. Liu, H. Zhang, L. Ma, H. Su, *Appl. Catal. B: Environ.* 218 (2017) 460–469.

[69] P. Liu, X. Gu, K. Kang, H. Zhang, J. Cheng, H. Su, *ACS Appl. Mater. Interfaces* 9 (2017) 10759–10767.

[70] R.D.L. Smith, M.S. Prévot, R.D. Fagan, Z. Zhang, P.A. Sedach, M.K.J. Siu, S. Trudel, C.P. Berlinguette, *Science* 340 (2013) 60–63.

[71] C.G. Morales-Guio, X. Hu, *Acc. Chem. Res.* 47 (2014) 2671–2681.

[72] H.R. Moon, D.-W. Lim, M.P. Suh, *Chem. Soc. Rev.* 42 (2013) 1807–1824.

[73] Q. Yang, Q. Xu, H.-L. Jiang, *Chem. Soc. Rev.* 46 (2017) 4774–4808.

[74] F. Dong, Z. Zhao, Y. Sun, Y. Zhang, S. Yan, Z. Wu, *Environ. Sci. Technol.* 49 (2015) 12432–12440.

[75] S. Jo, P. Verma, Y. Kuwahara, K. Mori, W. Choi, H. Yamashita, *J. Mater. Chem. A* 5 (2017) 21883–21892.